AGU100 ADVANCING EARTH AND SPACE SCIENCE

Geophysical Research Letters

RESEARCH LETTER
10.1029/2019GL086722

Dayside Field-Aligned Current Impacts on Ionospheric Irregularities

A. Fæhn Follestad[1], K. Herlingshaw[2,3], H. Ghadjari[4], D. J. Knudsen[4], K. A. McWilliams[5], J. I. Moen[1,2], A. Spicher[1], J. Wu[4], and Kjellmar Oksavik[2,3]

[1]Department of Physics, University of Oslo, Oslo, Norway, [2]The University Centre in Svalbard, Longyearbyen, Norway, [3]Birkeland Centre for Space Science, Department of Physics and Technology, University of Bergen, Bergen, Norway, [4]Department of Physics and Astronomy, University of Calgary, Calgary, Alberta, Canada, [5]Department of Physics and Engineering Physics, University of Saskatchewan, Saskatoon, Saskatchewan, Canada

Key Points:
- Severe GNSS phase scintillations in the winter dayside auroral ionosphere coincide with filamentary FACs
- Filamentary FACs appear to be essential for the creation of severe phase scintillations

Supporting Information:
- Supporting Information S1

Correspondence to:
A. Fæhn Follestad,
a.k.f.follestad@fys.uio.no

Citation:
Fæhn Follestad, A., Herlingshaw, K., Ghadjari, H., Knudsen, D. J., McWilliams, K. A., Moen, J. I., et al. (2020). Dayside field-aligned current impacts on ionospheric irregularities. *Geophysical Research Letters*, *47*, e2019GL086722. https://doi.org/10.1029/2019GL086722

Received 30 DEC 2019
Accepted 28 APR 2020
Accepted article online 7 MAY 2020

Abstract Global Navigation Satellite Systems (GNSS) are subject to disturbances caused by plasma irregularities in the ionosphere. Studies have suggested that in addition to the gradient drift and Kelvin-Helmholtz instabilities, electron precipitation may be important for phase scintillations in the dayside auroral region. This study combines in situ Swarm data with ground GNSS observations to investigate the potential role of filamentary field-aligned currents (FACs) on phase scintillations in the dayside auroral region by analyzing 22 events with phase scintillations exceeding 0.45 radians. We observe colocation between regions of severe phase scintillations and highly filamented FACs with fluctuations measured in the spacecraft frame of the order of 20 Hz. The observations indicate that filamentary FACs are crucial drivers for irregularities responsible for creating severe phase scintillations measured in the dayside auroral region and are thus of significant importance in the context of space weather impact on satellite communication.

Plain Language Summary Satellite-based navigation systems such as Global Positioning System (GPS) are known to be affected by dynamic phenomena in the upper atmosphere. The signals are subject to disturbances, resulting in reduced position accuracy or even a loss of signal reception. Several processes have been suggested as being responsible for these disturbances in the dayside auroral region, but their relative importance is still unclear. Thus, we used Swarm data as well as ground-based instrumentation to investigate this issue. We identified 22 events with severe disturbances that were located where we could compare data from the satellite and from ground-based instruments. We find that the occurrences of severe phase scintillation coincide with structured field-aligned currents (FACs), making them potentially a primary driver for signal disturbances in the daytime auroral region.

1. Introduction

Plasma irregularities with scale sizes ranging from a few meters to hundreds of kilometers are common in the cusp ionosphere (Basu et al., 1994, 1998; Moen et al., 2013; Spicher et al., 2017; Wernik et al., 2003). These irregularities can disrupt and disturb Global Navigation Satellite System (GNSS) signals through scintillations, that is, rapid fluctuations in phase and/or amplitude (Kintner et al., 2007, 2009, Yeh & Liu, 1982), degrading position accuracy and causing loss of lock (Aarons, 1982; Garner et al., 2011; Groves, 2013; Jacobsen & Andalsvik, 2016; Jin & Oksavik, 2018). GNSS systems are of increasing importance to global traffic and industry at high latitudes; thus, understanding ionospheric plasma irregularities in these regions is vital (e.g., Moen et al., 2013).

Two macroscale instability mechanisms are traditionally considered as being dominant in the creation of irregularities at high latitudes in the cusp inflow region (Carlson et al., 2007; Moen et al., 2013). Reconnection-driven flow shears make velocity shear mechanisms like the Kelvin-Helmholtz instability (KHI) a strong candidate for a plasma structuring mechanism (Basu et al., 1988,1990; Carlson, 2012, Keskinen et al., 1988, Oksavik et al., 2011), while plasma gradients, for example, associated with polar cap patches, provide conditions for the gradient drift instability (GDI) to develop (Moen et al., 2012; Ossakow & Chaturvedi, 1979; Tsunoda, 1988). Furthermore, these two instability modes may operate together in a two-step process (Carlson et al., 2007), in which the growth time of irregularities is faster than either one

separately. Statistical studies (e.g., Jin et al., 2015; Prikryl et al., 2015) have observed that phase scintillations on the dayside were closely colocated with the dayside auroral region.

Furthermore, evidence has been presented that the cusp particle precipitation itself may cause plasma irregularities on decameter to kilometer scales, either directly or indirectly by providing the conditions for GDI and KHI instabilities (Dyson et al., 1974; Dyson & Winningham, 1974; Fejer & Kelley, 1980; Labelle et al., 1989; Kelley et al., 1982; Moen et al., 2002, 2012). Later works by Jin et al. (2016, 2017b), Oksavik et al. (2017b), and van der Meeren et al. (2015) link phase scintillations on the dayside to the auroral cusp. The present study is motivated by recent observations by Clausen et al. (2016), who found that in the cusp region there was a significant enhancement in phase scintillations during periods of elevated field-aligned currents (FACs). Additionally, Jin et al. (2017b) analyzed a series of events with severe phase scintillations and concluded that phase scintillations in the cusp are strongest when both polar cap patches and cusp aurora are present.

The structuring of FACs may be visualized in the case of upward flowing current, where electron beams are discernable as auroral rays and other small-scale auroral features, which occur on scales as small as 70 m (Maggs & Davis, 1968; Borovsky et al., 1991). Several researchers (see, e.g., Chaston et al., 2011; Golovchanskaya et al., 2006; Swift, 1978) suggested that there is a relationship between the existence of discrete auroral arcs and turbulence in the magnetic (and electric) fields in the fine-scale FAC region.

The main motivation for this letter is to test the hypothesis that the presence of filamentary FACs is an essential component for the creation of severe phase scintillations on the dayside during winter time. For this, we combine data from a network of three GNSS receivers in Svalbard with in situ measurements obtained by the Swarm satellites and provide evidence that severe phase scintillations coincide with regions of filamentary FACs. Furthermore, the observations support that the filamentary FACs and precipitation can be the primary drivers for the creation of phase scintillation irregularities.

2. Instrumentation and Methodology

2.1. Swarm

The Swarm mission consists of three satellites (A, B, and C) launched by the European Space Agency in 2013. Swarm A and C orbit the Earth side by side at an initial altitude of 450 km and longitudinal separation 1–1.5°, while Swarm B orbits at an altitude of approximately 530 km (Friis-Christensen et al., 2008). In this study, we use plasma density measurements from the Langmuir Probe on the Electric Field Instrument (EFI) (Knudsen et al., 2017) and magnetic field measurements from the Vector Field Magnetometer (VFM, Olsen et al., 2013). From the Ionospheric Plasma IRregularities (IPIR) product (Jin et al., 2019), we use vertical total electron content (VTEC) as well as ROTI, which is the rate of change of VTEC index. We also include the rate of change of density index (RODI), which is the standard deviation of the rate of change of density computed in a 10 s running window. The VTEC, ROTI, and RODI all have a resolution of 1 Hz. For a detailed explanation of the IPIR data set, see Jin et al. (2019).

2.2. FAC Filamentation

As a proxy for FAC filamentation we use residual magnetic field components in the northward and eastward directions. The magnetic field data from the Swarm VFM instrument are provided in the North, East, Center (NEC) coordinate system at a resolution of 50 Hz. To calculate the residual magnetic field, we subtract the background magnetic field from each field component. The background magnetic field is calculated using a low-pass Savitzky-Golay filter with a window size of 15 s and an order of 3, as suggested by Park et al. (2017). This procedure allows to resolve structures in the magnetic field fluctuations with scale sizes up to 100 km.

The FAC density is related to the magnetic field as follows (Wang et al., 2005):

$$j_z = \frac{1}{\mu_0 v_x} \frac{\Delta B_y}{\Delta t}, \tag{1}$$

where v_x is the velocity perpendicular to the current sheet and ΔB_y is the residual magnetic component parallel to the current sheet. Thus, we consider fluctuations in the residual of the east component of the magnetic field to be indicators of filamentary FACs. To quantify small-scale magnetic field fluctuations, we present spectrograms exhibiting the power spectral density (PSD) with respect to time. To compute

the spectrograms, we use a fast Fourier transform and a running Hanning window with length of 6 s, at 1 s intervals (Welch, 1967).

2.3. GNSS Receivers

The University of Bergen operates three multiconstellation GNSS receivers located in and around Svalbard. The three receivers are located in Longyearbyen, Ny-Ålesund, and Bjørnøya and span geographic latitudes from 74.5° to 78.9°N and longitudes from 11.0° to 29.0°E (Oksavik et al., 2015). We use receiver data from GPS and its Russian counterpart GLONASS (GLObal NAvigation Satellite System) and apply a cutoff elevation angle of 25° to minimize multipath effects. In this study we use the conventional phase scintillation index σ_ϕ (Fremouw et al., 1978; Mushini et al., 2012; Rino, 1979; Van Dierendonck et al., 1993, 1996) with a resolution of 60 s. More information about the GNSS receiver network and data processing is found in Oksavik et al. (2015) and van der Meeren et al. (2015).

We tested scintillation data with a resolution of 1 s for the three cases presented in section 3. Comparing the plots with those in section 3, we see that the results do not change significantly. While the timing is superior with the 1 s data, it requires significantly more preprocessing. Since the 60 s σ_ϕ index is a commonly used output from the receiver and the results are supported by the 1 s σ_ϕ, we conclude that 60 s scintillation data are satisfactory for the purpose of this paper.

The index σ_ϕ is not always appropriate to determine diffractive contributions from ionospheric irregularities at high latitudes (McCaffrey & Jayachandran, 2019), as it may contain refractive contributions from larger scale irregularities (Beach, 2006; Forte & Radicella, 2004; McCaffrey & Jayachandran, 2019; Wang et al., 2018). Here, however, we are not attempting to discern between refractive or diffractive effects.

2.4. SuperDARN

The Super Dual Auroral Radar Network (SuperDARN) is a network of over 30 high-frequency coherent radars designed to study *F* region plasma drift (Chisham et al., 2007; Greenwald et al., 1995). Individual radars can measure the line-of-sight convection velocity, spectral width, and backscattered power from the field-aligned irregularities. This study uses data from the Hankasalmi radar, located at 62.32°N, 26.61°E.

2.5. Ionospheric Piercing Point Methodology

We need a criterion to judge which ground-based observations are within a reasonable distance and time from the Swarm satellite to be able to make a comparison. We estimate the position of the ionospheric piercing point (IPP), based on the receiver location and elevation and azimuth angle of the tracked GNSS satellite, and assuming that the ionosphere is projected to 350 km altitude. For each time step, we calculate the distance between the position of Swarm and the IPP, D, to judge whether the satellite is within a reasonable distance in time and space from an IPP, which we set to $D \leq 110$ km (a distance corresponding to about 1° latitude in the polar regions). The method is illustrated in Figure 1a. Here, we show the Swarm trajectory (black line) with timestamps. The black cross (x) is Swarm's position at 09:09 UT, and the black circle has a radius of 110 km. For each 1 s time step t, we look for receiver data within a time period $t \pm 30$ s, for which we calculate IPP coordinates and D. We evaluate the phase scintillation values at all piercing points within $D \leq 110$ km and record the maximum phase scintillation value as the phase scintillation level for that time step. We repeat the procedure for each time step.

2.6. Data Set

This study considers data from the period September 2014 to December 2017. We include only events that are between the months of November through March, because phase scintillations are stronger in local winter in the Northern Hemisphere cusp (Jin et al., 2018; Kersley et al., 1995; Prikryl et al., 2011, 2015; Skone et al., 2008). Additionally, we only consider events between 06 and 12 UT, corresponding to approximately 8.5 to 14.5 magnetic local time, during which Svalbard is near the dayside auroral region. In total, 80 events were identified to include conjunctions between the presence of significant phase scintillations based on data from the ground based GNSS receivers at Svalbard and at least one Swarm satellite pass. We compare data from different instruments as outlined above.

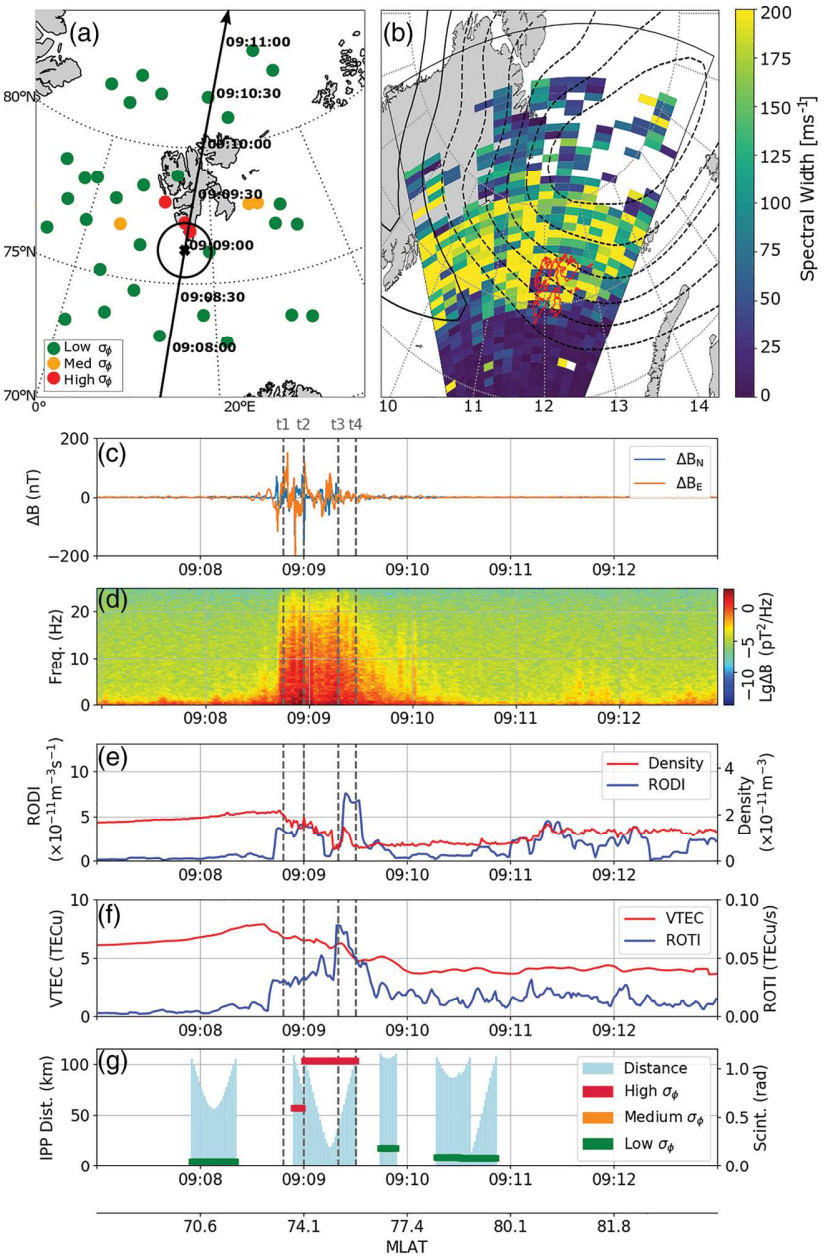

Figure 1. (a) Map of Svalbard with Swarm B trajectory and labeled timestamps. The black circle indicates 110 km radius around Swarm at 09:09 UT. Phase scintillations are shown as red (≥0.45 rad), orange ($0.25 \leq \sigma_\phi < 0.45$ rad), and green (<0.25 rad) dots. (b) The spectral width values (in MLT/MLAT coordinates) measured by the Hankasalmi SuperDARN radar at 09:09 UT where dashed and solid contours represent equipotential contours of the global convection flow. Svalbard is outlined in red for clarity. (c–e) Time series for 24 October 2014, 09:07–09:12 UT. (c and d) ΔB and its PSD, respectively. (e) The plasma density (right-hand axis) and RODI derived from Swarm Langmuir Probe data (left-hand axis). (f) Vertical total electron content (VTEC) in terms of TECu on the left-hand-side axis (red line), and the rate of change of VTEC index (ROTI) on the right-hand-side axis (blue line), in units TECu/s. Both VTEC and RODI are from the Swarm IPIR data set. (g) The phase scintillation values, using the same color-coding as in (a). The blue shading indicates distance from Swarm to the IPP, plotted on the left-hand-side axis. Four time stamps ($t_1 - t_4$) are indicated with vertical dashed gray lines to facilitate discussion.

3. Results

3.1. General

From our initial data set of 80 events, we analyze further only those that contain severe phase scintillations in the vicinity of Swarm (see section 2.5). The threshold for severe phase scintillations is set to $\sigma_\phi \geq 0.45$ radians, which reduces the data set to 22 events. Traditionally, phase scintillations above 0.5 radians are considered severe (Skone et al., 2005), but we chose to relax this threshold to 0.45 radians to give us a larger sample size for analysis. Indeed, performing the same analysis using a threshold of 0.5 radians, our data set was reduced to only 15 events, but exhibiting similar results as the ones presented below.

We made stacked plots of magnetic field perturbations (ΔB) and their PSDs, plasma density variation index (RODI), TEC variation index (ROTI), and phase scintillations. The stacked plots allowed us to analyze the events and compare phase scintillation indices with those quantities. Out of the 22 events, we find severe scintillations to be located in regions with filamentary FACs in 21 cases. Fifteen events had both elevated ΔB and RODI colocated with severe phase scintillations. There were six cases that had elevated ΔB but negligible RODI and ROTI levels together with severe phase scintillations. We identified one occurrence of severe phase scintillations that were only partially colocated with the region of filamentary FAC (Figure S16 in the supporting information). However, the same case shows definitive colocation with filamentary FACs if we decrease the IPP altitude parameter to 250 km. We therefore conclude that this example does not contradict our hypothesis. It is also worth mentioning that similar general results were obtained by changing the IPP altitutde to 250 and 450 km, and the distance D, as described in section 2.5.

The entire data set of 22 cases is included in the supporting information. In the following section, we present three typical cases to illustrate events where filamentary FACs are colocated with phase scintillations.

3.2. Case Study

The first event takes place on 24 October 2014 09:07–09:13 UT. Solar wind data retrieved from the OMNIweb service (King & Papitashvili, 2005) showed that for a period of 50 min before the severe phase scintillations observed at 09:09 UT, the IMF was stable with average values of $B_Z \sim -3.1$ nT and $B_Y \sim 3.7$ nT (Geocentric Solar Magnetic [GSM] coordinates). The global convection pattern (see Figure 1b) has a twin cell configuration consistent with negative B_Z and the expected asymmetry due to positive IMF B_Y.

Figure 1 contains plots from the 24 October 2014 event, centered on 09:10 UT. Figure 1a is a map where the trajectory of Swarm B is indicated with a black line. The time stamps (in UT) are labeled. The colored dots are phase scintillation levels at different IPPs for one time instant, 09:09 UT. Red dots indicate severe phase scintillations (≥0.45 rad), orange dots are medium phase scintillations ($0.25 \leq \sigma_\phi < 0.45$ rad), and green dots are low-phase scintillations (<0.25 rad). The circle represents the maximum D (110 km) for one time step, at 09:09 UT.

Figure 1b shows the spectral width measurements from the Hankasalmi SuperDARN radar, which contain high values of 200 m s^{-1}, indicating that the flow is disturbed, either by turbulence, large-scale velocity shears, or structured precipitation (Chisham et al., 2007, and references therein). The radar measurements put the Swarm observations into context, showing that Swarm is encountering the postnoon cusp inflow region.

Figure 1c shows time series of the magnetic field perturbations (ΔB) in northward (blue) and eastward (orange) directions. We have marked four times of interest and labeled them t_1 through t_4. Before t_1 perturbations in ΔB are low. At t_1 we see a sharp increase in both the eastward and northward perturbation, with local maxima around t_2. The perturbations subside slowly and return to a background level around t_4. Figure 1d shows the PSD time series of the residual eastward magnetic field, where the color scale is logarithmic. Before t_1 there are only slow variations in the magnetic field perturbations, of the order of 1 Hz. At t_1 there is a sharp increase in intensity over the whole frequency range, where the fluctuations reach up to 20 Hz, corresponding to a scale size of 400 m along Swarm's trajectory. The intensification subsides slowly over the next minute and returns to normal levels shortly after t_4.

Figure 1e shows the RODI time series based on Swarm data plotted in blue (left-hand axis) and the plasma density in red (right-hand axis). Before t_1 the plasma density is steady and relatively high at around 1.8×10^5 cm^{-3}, and RODI is accordingly low. At t_1 the plasma density starts to decline, accompanied by an increase in RODI. This implies that Swarm is now at the poleward edge of the dayside sunlit plasma reservoir. The

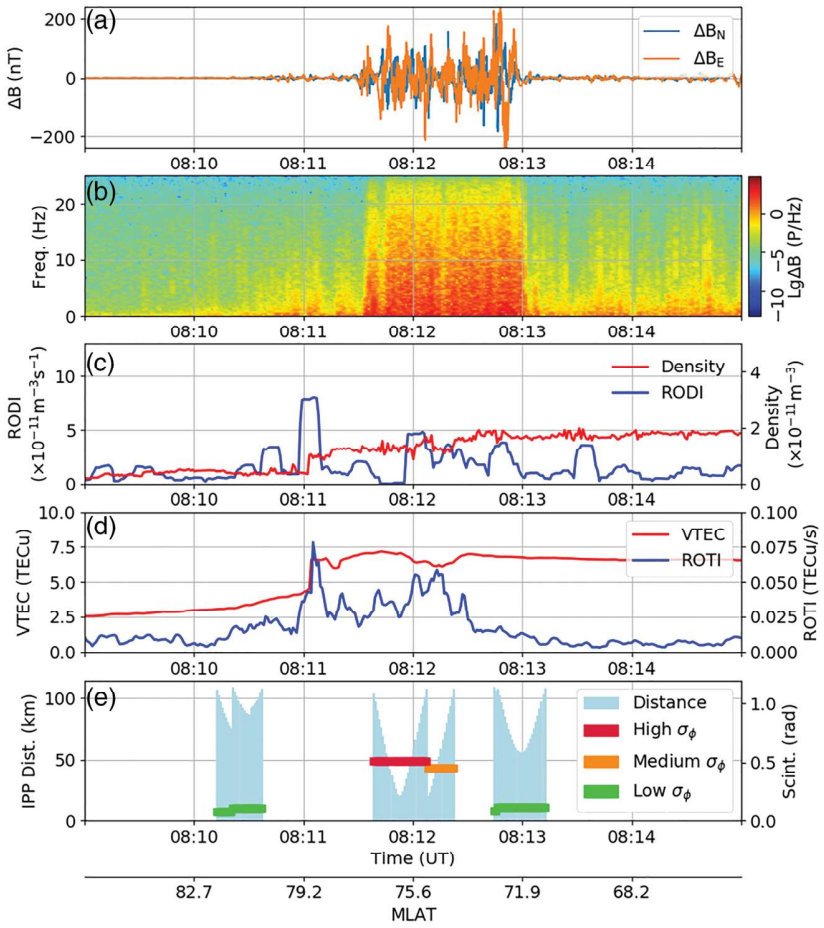

Figure 2. (a–d) Data from Swarm A, 3 November 2015 08:10–08:14 UT. (a) Magnetic field perturbations, (b) PSD of magnetic field perturbations, (c) Plasma density/RODI time series, (d) VTEC/ROTI time series, and (e) phase scintillations. The plots correspond to (c)–(g) of the Figure 1 caption.

plasma density continues to decrease before it stabilizes around 0.5×10^5 cm^{-3} at t_4. Both the RODI and density have a spike at time t_3. After t_4 the plasma density and RODI vary slightly inside the polar cap.

Figure 1f shows Swarm's estimated VTEC (red line) and ROTI (blue line) from Swarm's GPS receiver on the right axis. VTEC paints a picture that is very similar to that inferred from the plasma density data from Figure 1e. ROTI, which when enhanced is traditionally associated with enhanced phase scintillations (Basu et al., 1999; Jacobsen & Dahnn, 2014; Jacobsen & Andalsvik, 2016), shows a significant peak at t_4 and enhanced values over the entire cusp region.

Figure 1g shows the phase scintillation time series with the same color-coding as in Figure 1a. Additionally, we have included a shaded background that indicates distance D from Swarm to the IPP, with the scale plotted on the left-hand-side axis. Note that D cannot exceed 110 km. Before t_1 we observe some very low level phase scintillations at 09:08 UT. At t_2 Swarm is within 110 km of a second piercing point, which gives phase scintillation values of 1 radian. After t_4 the phase scintillation levels drop significantly. By comparing Figure 1c–Figure 1e, with Figure 1g, it is clear that the severe phase scintillations coincide with the region of structured FAC, and the enhanced density variations are observed between t_1 and t_3.

We now present two additional events, which highlight different situations in which we find colocation between filamentary FACs and severe phase scintillations. Figure 2 shows an event where the observed filamentary FACs occur inside the region with very slowly decreasing electron density, with colocated phase scintillation measurements. At the beginning of the event, Swarm A is located in the polar cap and orbits

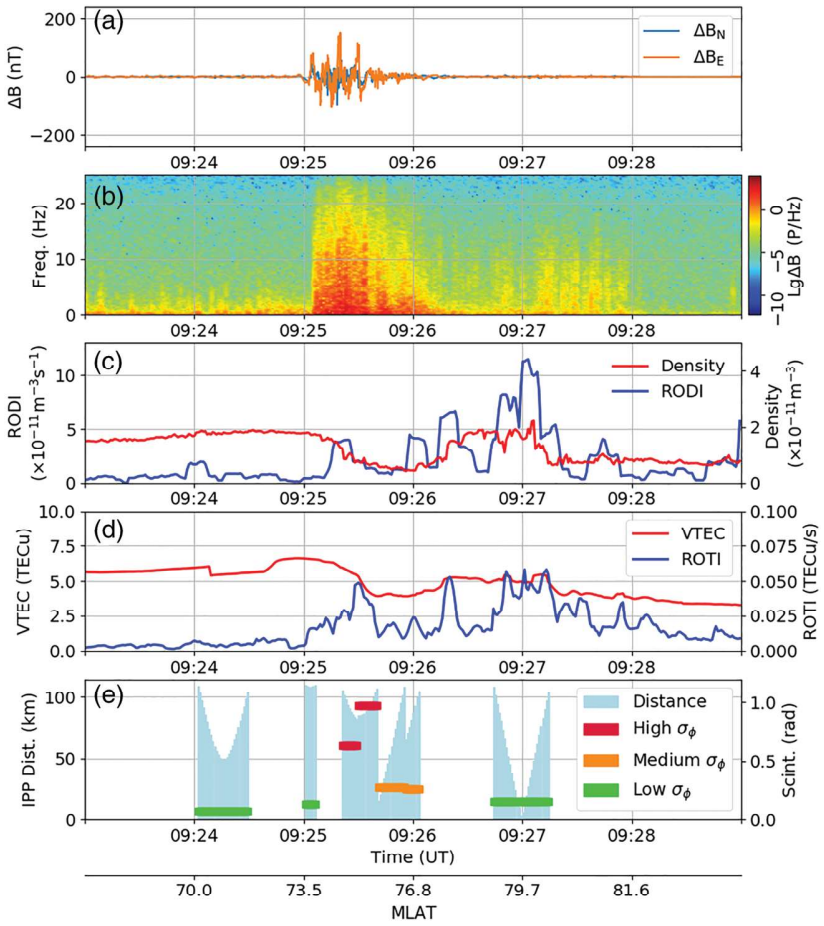

Figure 3. (a–d) Data from Swarm B, 23 October 2014, 09:22–09:28 UT. (a) Magnetic field perturbations, (b) PSD of magnetic field perturbations, (c) plasma density/RODI time series, (d) VTEC/ROTI time series, and (e) phase scintillations. The plots correspond to (c)–(g) of the Figure 1 caption.

toward lower latitudes on the dayside from about 08:11 UT. While Swarm is inside a broad region of filamentary FACs, which lasts from around 08:11:30 to 08:13:00 UT and corresponds to about 675 km, the plasma density is fairly stable around 1.2–1.8 $\times 10^5 \mathrm{cm}^{-3}$. The density fluctuations observed do not seem to be associated with a polar cap patch, nor any large-scale density enhancements.

Figure 3 shows Swarm and phase scintillation data from Swarm B on 23 October 2014, 09:22 to 09:28 UT, in the same format as the previous figures. Swarm traverses the dayside auroral zone between 09:25 and 09:26 UT, as evident by the structuring in ΔB shown in Figures 3a and 3b at this time. The plasma density time series (Figure 3c) shows that Swarm passes from inside the sunlit EUV region and into the polar cap at approximately 09:25:30 UT, where a sharp plasma density gradient is visible together with local maxima in ROTI and RODI. Comparing Figures 3c–3e, we note that there are severe phase scintillations colocated with the filamentary FACs between 09:25 and 09:26 UT in the region of density decrease. After 09:26 UT, Swarm is inside the polar cap. Around 09:27 UT, we observe several large enhancements in RODI and ROTI. High levels of ROTI and RODI indicate the presence of strong plasma density gradients; however, phase scintillation levels are very low at this instant in time.

4. Discussion

In this study, we take advantage of in situ measurements by the Swarm satellites and GNSS receiver network in Svalbard to investigate the driver for severe phase scintillations on the dayside during the winter months. Observations showed that severe phase scintillations consistently coincided with the presence of filamentary

FACs. Among all cases, five events showed colocation of filamentary FACs and severe phase scintillation levels without the presence of large plasma density gradients.

The study presented in this paper has an element of uncertainty related to the geometry of observations. The locations of regions that contribute to scintillations measured on the ground depend on the assumed IPP altitude and the elevation of the tracked GNSS satellite. When comparing the time series, an adjustment in IPP altitude translates to a shift in time along Swarm's trajectory especially for IPPs with line of sight parallel to the orbit. A sensitivity analysis investigating the effects of changing the IPP parameter to 250 and 450 km has therefore been carried out. Out of all the events, only one did not show severe scintillations exactly colocated with filamentary FACs for an IPP altitude of 250 km, but it did show colocation for IPP altitudes 350 and 450 km. This event and the one mentioned in section 3.1 are therefore ambiguous, as we cannot know which altitude is most correct for each one. We have also tested the importance of maximum distance D from the IPP coordinate to Swarm's trajectory. In two trial runs, we have reduced maximum D to 75 km and then increased it to 150 km. The scintillation time series changes somewhat, but not enough to alter the final conclusion. The data set showed coherent results between all three IPP altitudes and distances. We therefore conclude that our method demonstrates consistent colocation between regions of filamentary FACs and severe phase scintillations in the winter time cusp.

The case studies summarized in Figures 1 and 3 show evidence of phase scintillations colocated with filamentary FACs on the boundary between the sunlit dayside plasma reservoir and the low plasma density in the polar cap. In Case 1, there are also high spectral widths in SuperDARN echoes, as well as a small spike in RODI and ROTI. We cannot exclude that the GDI and/or KHI are at work in these events, and the KHI could structure the plasma on which the GDI could further create small-scale irregularities as suggested by Carlson et al. (2007). In Case 3, we observe a large enhancement in RODI about 1 min after the filamentary FACs have subsided, which does not result in severe scintillations on the ground. This example agrees with previous findings (Clausen et al., 2016; Jin et al., 2017a) that report that patches inside the polar cap are less of a space weather threat than patches in the auroral oval and that filamentary FACs act as a driver for irregularities in the cusp. It is worth mentioning that geometrical effects may be important here, as the line of sight may only intersect part of the irregularities. The elevation angle was about 35° at the time shown in Case 3, and no severe phase scintillations were observed around that latitude before or after for at least 20 min. For Case 2 (Figure 2), there are no strong density gradients in the region of severe scintillations. This is a strong indicator that the irregularities causing phase scintillations are produced by filamentary FACs and the associated precipitating electrons. It has been suggested that cusp precipitation may initialize the GDI (Moen et al., 2012). Therefore, it is difficult to assess the role of each process, but it is clear that the phase scintillations are colocated with filamentary FACs.

After careful examination of the entire data set, we discuss a hypothesis for how filamentary FACs produce severe phase scintillations in the cusp. The filamentary FACs can cause severe phase scintillations through the production of plasma density irregularities, which may work through direct driving of the ionospheric plasma by structured precipitation and/or electric fields (Millward et al., 1999; Moen et al., 2002, 2012). Additionally, the FACs can work as enablers for the GDI and/or KHI, by providing the initial perturbation by the inflow of electrons (Kelley et al., 1982; Moen et al., 2012). Lastly, these mechanisms can work in combination. The structuring in the FACs thus results in plasma density variations in the direction perpendicular to the ambient magnetic field (e.g., Dyson, 1974; Millward et al., 1999; Moen et al., 2002, 2012).

Going forward, it would be interesting to conduct a more detailed analysis at higher resolution and using multiple observations from different lines of sight, for example, as demonstrated by Mrak et al. (2018). It would also be interesting to consider the relationship between filamentation scale size and scintillation intensity and investigate the difference between upward and downward FACs with respect to phase scintillations. For this, precise geometry and timing would be required. The Grand Challenge Initiative Cusp Rockets (Moen et al., 2018) will provide high-resolution data that can improve the analysis. This would provide valuable understanding of the filamentary FACs' role in producing scintillation in the dayside auroral region.

5. Conclusion

This paper has presented evidence that filamentary FACs are colocated with severe phase scintillation in the dayside auroral region. We analyzed Swarm data from 22 passes through the winter dayside auroral

region that show severe phase scintillations over Svalbard. Analysis showed that in all events with severe phase scintillations, there is evidence of colocated filamentary FACs. In contrast, large-density gradients were present in only 15 out of the 22 events studies. This finding strongly suggests that filamentary FACs are an essential component for phase scintillations in the dayside auroral region. For space weather research, the role of electron precipitation in generating phase scintillations in the dayside auroral region has significant implications.

Acknowledgments
The work would not have been possible without Canada-Norway mobility funds provided by the Norwegian Agency for International Cooperation and Quality Enhancement in Higher Education, Project NNA-2016/10081. J. M. and A. S. received funding from the Research Council of Norway Grant 275653. K. O. received funding from the Research Council of Norway Grants 212014 and 223252. We acknowledge the use of NASA/GSFC's Space Physics Data Facility's CDAWeb and ftp services and OMNI data. Swarm is a European Space Agency mission with major support from the Canadian Space Agency for the EFI. Swarm data can be accessed from ESA's data access webpage (https://earth.esa.int/web/guest/swarm/data-access). The authors acknowledge the use of SuperDARN data. SuperDARN is a collection of radars funded by national scientific funding agencies of Australia, Canada, China, France, Japan, South Africa, United Kingdom, and United States of America. We also thank Mark Lester, the PI of the Hankasalmi radar for use of the data. SuperDARN data are available from the British Antarctic Survay (at https://www.bas.ac.uk/project/superdarn/). Scintillation data from GPS and GLONASS were provided by Kjellmar Oksavik, University of Bergen (kjellmar.oksavik@uib.no). The scintillation data have been published in Mendeley Data and are available online (at https://doi.org/10.17632/vzgv93rr8z.2).

References

Aarons, J. (1982). Global morphology of ionospheric scintillations. *Proceedings of the IEEE*, *70*(4), 360–378. https://doi.org/10.1109/PROC.1982.12314

Basu, S., Basu, Su., Chaturvedi, P. K., & Bryant Jr., C. M. (1994). Irregularity structures in the cusp/cleft and polar cap regions. *Radio Science*, *29*(1), 195–207. https://doi.org/10.1029/93RS01515

Basu, S., Basu, S., MacKenzie, E., Coley, W. R., Sharber, J. R., & Hoegy, W. R. (1990). Plasma structuring by the gradient drift instability at high latitudes and comparison with velocity shear driven processes. *Journal of Geophysical Research*, *95*(A6), 7799–7818. https://doi.org/10.1029/JA095iA06p07799

Basu, S., Basu, S., MacKenzie, E., Fougere, P. F., Coley, W. R., Maynard, N. C., et al. (1988). Simultaneous density and electric field fluctuation spectra associated with velocity shears in the auroral oval. *Journal of Geophysical Research*, *93*(A1), 115–136. https://doi.org/10.1029/JA093iA01p00115

Basu, S, Groves, K. M, Quinn, J. M, & Doherty, P (1999). A comparison of TEC fluctuations and scintillations at ascension island. *Journal of Atmospheric and Solar-Terrestrial Physics*, *61*(16), 1219–1226. https://doi.org/10.1016/S1364-6826(99)00052-8

Basu, S., Weber, E. J., Bullett, T. W., Keskinen, M. J., MacKenzie, E., Doherty, P., et al. (1998). Characteristics of plasma structuring in the cusp/cleft region at Svalbard. *Radio Science*, *33*(6), 1885–1899. https://doi.org/10.1029/98RS01597

Beach, T. L. (2006). Perils of the GPS phase scintillation index. *Radio Science*, *41*, RS5S31.

Borovsky, J. E., Suszcynsky, D. M., Buchwald, M. I., & DeHaven, H. V. (1991). Measuring the thicknesses of auroral curtains. *Arctic*, 231–238.

Carlson, H. C. (2012). Sharpening our thinking about polar cap ionospheric patch morphology, research, and mitigation techniques. *Radio Science*, *47*, RS0L21.

Carlson, H. C., Pedersen, T., Basu, S., Keskinen, M., & Moen, J. (2007). Case for a new process, not mechanism, for cusp irregularity production. *Journal of Geophysical Research*, *112*, A11304. https://doi.org/10.1029/2007JA012384

Chaston, C. C., Seki, K, Sakanoi, T, Asamura, K., & Hirahara, M (2011). Evidence for a multi-scale aurora, *The dynamic magnetosphere* (pp. 271–280). Dordrecht, Netherlands: Springer.

Chisham, G., Lester, M., Milan, S. E., Freeman, M. P., Bristow, W. A., Grocott, A., et al. (2007). A decade of the Super Dual Auroral Radar Network (SuperDARN): Scientific achievements, new techniques and future directions. *Surveys in Geophysics*, *28*(1), 33–109. https://doi.org/10.1029/98RS01597

Clausen, L. B. N., Moen, J. I., Hosokawa, K., & Holmes, J. M. (2016). GPS scintillations in the high latitudes during periods of dayside and nightside reconnection. *Journal of Geophysical Research: Space Physics*, *121*, 3293–3309. https://doi.org/10.1002/2015JA022199

Dyson, P. L., McClure, J. P., & Hanson, W. B. (1974). In situ measurements of the spectral characteristics of F region ionospheric irregularities. *Journal of Geophysical Research*, *79*(10), 1497–1502. https://doi.org/10.1029/JA079i010p01497

Dyson, P. L., & Winningham, J. D. (1974). Top side ionospheric spread F and particle precipitation in the day side magnetospheric clefts. *Journal of Geophysical Research*, *79*(34), 5219–5230. https://doi.org/10.1029/JA079i034p05219

Fejer, B. G, & Kelley, M. C. (1980). Ionospheric irregularities. *Reviews of Geophysics*, *18*(2), 401–454. https://doi.org/10.1029/RG018i002p00401

Forte, B., & Radicella, S. M. (2004). Geometrical control of scintillation indices: What happens for GPS satellites. *Radio Science*, *39*, RS5014.

Fremouw, E. J., Leadabrand, R. L., Livingston, R. C., Cousins, M. D., Rino, C. L., Fair, B. C., & Long, R. A. (1978). Early results from the DNA wideband satellite experiment complex-signal scintillation. *Radio Science*, *13*(1), 167–187. https://doi.org/10.1029/RS013i001p00167

Friis-Christensen, E., Lhr, H., Knudsen, D., & Haagmans, R. (2008). Swarm—An Earth observation mission investigating geospace. *Advances in Space Research*, *41*(1), 210–216. https://doi.org/10.1016/j.asr.2006.10.008

Garner, T. W., Harris, R. B., York, J. A., Herbster, C. S., Minter III, C. F., & Hampton, D. L. (2011). An auroral scintillation observation using precise, collocated GPS receivers. *Radio Science*, *46*, RS1018. https://doi.org/10.1029/2010RD004412

Golovchanskaya, I. V., Ostapenko, A. A., & Kozelov, B. V. (2006). Relationship between the high-latitude electric and magnetic turbulence and the Birkeland field-aligned currents. *Journal of Geophysical Research*, *111*, A12301. https://doi.org/10.1029/2006JA011835

Greenwald, R. A., Baker, K. B., Dudeney, J. R., Pinnock, M., Jones, T. B., Thomas, E. C., et al. (1995). DARN/SuperDARN. *Space Science Reviews*, *71*(1), 761–796. https://doi.org/10.1007/bf00751350

Groves, P. D. (2013). *Principles of GNSS, inertial, and multisensor integrated navigation systems*. Boston/London: Artech House.

Jacobsen, K. S., & Andalsvik, Y. L. (2016). Overview of the 2015 St. Patrick's day storm and its consequences for RTK and PPP positioning in Norway. *Journal Space Weather Space Climate*, *6*, A9. https://doi.org/10.1051/swsc/2016004

Jacobsen, K. S., & Dahnn, M. (2014). Statistics of ionospheric disturbances and their correlation with GNSS positioning errors at high latitudes. *Journal Space Weather Space Climate*, *4*, A27. https://doi.org/10.1051/swsc/2014024

Jin, Y., Miloch, W. J., Moen, J. I., & Clausen, L. B. N. (2018). Solar cycle and seasonal variations of the GPS phase scintillation at high latitudes. *Journal Space Weather Space Climate*, *8*, A48. https://doi.org/10.1051/swsc/2018034

Jin, Y., Moen, J. I., & Miloch, W. J. (2015). On the collocation of the cusp aurora and the GPS phase scintillation: A statistical study. *Journal of Geophysical Research: Space Physics*, *120*, 9176–9191. https://doi.org/10.1002/2015JA021449

Jin, Y., Moen, J. I., Miloch, W. J., Clausen, L. B. N., & Oksavik, K. (2016). Statistical study of the GNSS phase scintillation associated with two types of auroral blobs. *Journal of Geophysical Research: Space Physics*, *121*, 4679–4697. https://doi.org/10.1002/2016JA022613

Jin, Y., Moen, J. I., Oksavik, K., Spicher, A., Clausen, L. B., & Miloch, W. J. (2017). GPS scintillations associated with cusp dynamics and polar cap patches. *Journal of Space Weather and Space Climate*, *7*, A23.

Jin, Y., Moen, J. I., Oksavik, K., Spicher, A., Clausen, L. B. N., & Miloch, W. J. (2017). GPS scintillations associated with cusp dynamics and polar cap patches. *Journal of Space Weather and Space Climate*, *7*, A23.

Jin, Y., & Oksavik, K. (2018). GPS scintillations and losses of signal lock at high latitudes during the 2015 St. Patrick's day storm. *Journal of Geophysical Research: Space Physics*, *123*, 7943–7957. https://doi.org/10.1029/2018JA025933

Jin, Y., Spicher, A., Xiong, C., Clausen, L. B. N., Kervalishvili, G., Stolle, C., & Miloch, W. J. (2019). Ionospheric plasma irregularities characterized by the Swarm satellites: Statistics at high latitudes. *Journal of Geophysical Research: Space Physics*, *124*, 1262–1282. https://doi.org/10.1029/2018JA026063

Kelley, M. C., Vickrey, J. F., Carlson, C. W., & Torbert, R. (1982). On the origin and spatial extent of high-latitude F region irregularities. *Journal of Geophysical Research*, *87*(A6), 4469–4475. https://doi.org/10.1029/JA087iA06p04469

Kersley, L., Russell, C. D., & Rice, D. L. (1995). Phase scintillation and irregularities in the northern polar ionosphere. *Radio Science*, *30*(3), 619–629. https://doi.org/10.1029/94RS03175

Keskinen, M. J., Mitchell, H. G., Fedder, J. A., Satyanarayana, P., Zalesak, S. T., & Huba, J. D. (1988). Nonlinear evolution of the Kelvin-Helmholtz instability in the high-latitude ionosphere. *Journal of Geophysical Research*, *93*(A1), 137–152. https://doi.org/10.1029/JA093iA01p00137

King, J., & Papitashvili, N. (2005). Solar wind spatial scales in and comparisons of hourly Wind and ACE plasma and magnetic field data. *Journal of Geophysical Research*, *110*, A02104. https://doi.org/10.1029/2004JA010649

Kintner, P. M., Humphreys, T., & Hinks, J. (2009). GNSS and ionospheric scintillation. *Inside GNSS*, *4.4*, 22–30.

Kintner, P. M., Ledvina, B. M., & Paula, E. R. (2007). GPS and ionospheric scintillations. *Space Weather*, *5*, S09003. https://doi.org/10.1029/2006SW000260

Knudsen, D. J., Burchill, J. K., Buchert, S. C., Eriksson, A. I., Gill, R., Wahlund, J.-E., et al. (2017). Thermal ion imagers and Langmuir probes in the Swarm electric field instruments. *Journal of Geophysical Research: Space Physics*, *122*, 2655–2673. https://doi.org/10.1002/2016JA022571

Labelle, J., Sica, R. J., Kletzing, C., Earle, G. D., Kelley, M. C., Lummerzheim, D., et al. (1989). Ionization from soft electron precipitation in the auroral F region. *Journal of Geophysical Research*, *94*(A4), 3791–3798. https://doi.org/10.1029/JA094iA04p03791

Maggs, J., & Davis, T. (1968). Measurements of the thicknesses of auroral structures. *Planetary and Space Science*, *16*(2), 205–209.

McCaffrey, A., & Jayachandran, P. (2019). Determination of the refractive contribution to GPS phase scintillation. *Journal of Geophysical Research: Space Physics*, *124*, 1454–1469. https://doi.org/10.1029/2018JA025759

Millward, G. H., Moffett, R. J., Balmforth, H. F., & Rodger, A. S. (1999). Modeling the ionospheric effects of ion and electron precipitation in the cusp. *Journal of Geophysical Research*, *104*(A11), 24,603–24,612. https://doi.org/10.1029/1999JA900249

Moen, J., Oksavik, K., Abe, T., Lester, M., Saito, Y., Bekkeng, T. A., & Jacobsen, K. S. (2012). First in-situ measurements of HF radar echoing targets. *Geophysical Research Letters*, *39*, L07104. https://doi.org/10.1029/2012GL051407

Moen, J., Oksavik, K., Alfonsi, L., Daabakk, Y., Romano, V., & Spogli, L. (2013). Space weather challenges of the polar cap ionosphere. *Journal Space Weather Space Climate*, *3*, A02.

Moen, J., Spicher, A., Rowland, D., Kletzing, C., & LaBelle, J. (2018). Grand challenge initiative-cusp: Rockets to explore solar wind-driven dynamics of the top side polar atmosphere. In *SESS 2018 The State of Environmental Science in Svalbard* (pp. 184–204). Longyearbyen: Svalbard Integrated Arctic Earth Observing System.

Moen, J., Walker, I. K., Kersley, L., & Milan, S. E. (2002). On the generation of cusp HF backscatter irregularities. *Journal of Geophysical Research*, *107*(A4), L07104. https://doi.org/10.1029/2001JA000111

Mrak, S., Semeter, J., Hirsch, M., Starr, G., Hampton, D., Varney, R. H., et al. (2018). Field-aligned GPS scintillation: Multisensor data fusion. *Journal of Geophysical Research: Space Physics*, *123*, 974–992. https://doi.org/10.1002/2017JA024557

Mushini, S. C., Jayachandran, P., Langley, R., MacDougall, J., & Pokhotelov, D (2012). Improved amplitude-and phase-scintillation indices derived from wavelet detrended high-latitude GPS data. *GPS solutions*, *16*(3), 363–373.

Oksavik, K., Moen, J. I., Rekaa, E. H., Carlson, H. C., & Lester, M. (2011). Reversed flow events in the cusp ionosphere detected by SuperDARN HF radars. *Journal of Geophysical Research*, *116*, A12303. https://doi.org/10.1029/2011JA016788

Oksavik, K., van der Meeren, C., Lorentzen, D. A., Baddeley, L. J., & Moen, J. (2015). Scintillation and loss of signal lock from poleward moving auroral forms in the cusp ionosphere. *Journal of Geophysical Research: Space Physics*, *120*, 9161–9175. https://doi.org/10.1002/2015JA021528

Olsen, N., Friis-Christensen, E., Floberghagen, R., Alken, P., Beggan, C. D., Chulliat, A., et al. (2013). The Swarm satellite constellation application and research facility (SCARF) and Swarm data products. *Earth, Planets and Space*, *65*(11), 1.

Ossakow, S. L., & Chaturvedi, P. K. (1979). Current convective instability in the diffuse aurora. *Geophysical Research Letters*, *6*(4), 332–334. https://doi.org/10.1029/GL006i004p00332

Park, J., Lhr, H., Knudsen, D. J., Burchill, J. K., & Kwak, Y.-S. (2017). Alfvn waves in the auroral region, their poynting flux, and reflection coefficient as estimated from swarm observations. *Journal of Geophysical Research: Space Physics*, *122*, 2345–2360. https://doi.org/10.1002/2016JA023527

Prikryl, P., Jayachandran, P. T., Chadwick, R., & Kelly, T. D. (2015). Climatology of GPS phase scintillaiton at northern high latitudes for the period from 2008 to 2013. *Annales Geophysicae*, *33*, 531–545. https://doi.org/10.5194/angeo-33-531-2015

Prikryl, P., Jayachandran, P. T., Mushini, S. C., & Chadwick, R. (2011). Climatology of GPS phase scintillation and HF radar backscatter for the high-latitude ionosphere under solar minimum conditions. *Annales Geophysicae*, *29*(2), 377–392. https://doi.org/10.5194/angeo-29-377-2011

Rino, C. L. (1979). A power law phase screen model for ionospheric scintillation: 1. Weak scatter. *Radio Science*, *14*(6), 1135–1145. https://doi.org/10.1029/RS014i006p01135

Skone, S, Feng, M, Ghafoori, F, & Tiwari, R (2008). Investigation of scintillation characteristics for high latitude phenomena. In *Proc. ion gnss*, pp. 2425–2433.

Skone, S, Lachapelle, G, Yao, D, Yu, W, & Watson, R (2005). Investigating the impact of ionospheric scintillation using a GPS software receiver. In *Proc. ion gnss*, pp. 1126–1137.

Spicher, A., Clausen, L. B. N., Miloch, W. J., Lofstad, V., Jin, Y., & Moen, J. I. (2017). Interhemispheric study of polar cap patch occurrence based on Swarm in situ data. *Journal of Geophysical Research: Space Physics*, *122*, 3837–3851. https://doi.org/10.1002/2016JA023750

Swift, D. W. (1978). Mechanisms for the discrete aurora—A review. *Space Science Reviews*, *22*(1), 35–75.

Tsunoda, R. (1988). High-latitude F-region irregularities: A review and synthesis. *Reviews of Geophysics*, *26*(4), 719–760. https://doi.org/10.1029/RG026i004p00719

Van Dierendonck, A., Hua, Q., Fenton, P., & Klobuchar, J. (1996). Commercial ionospheric scintillation monitoring receiver development and test results. Navigation technology for the 3 rd millennium 573–582.

Van Dierendonck, A., Klobuchar, J., & Hua, Q. (1993). Ionospheric scintillation monitoring using commercial single frequency C/A code receivers. In *proceedings of ION GPS*, *93*, pp. 1333–1342.

van der Meeren, C., Oksavik, K., Lorentzen, D. A., Rietveld, M. T., & Clausen, L. B. N. (2015). Severe and localized GNSS scintillation at the poleward edge of the nightside auroral oval during intense substorm aurora. *Journal of Geophysical Research: Space Physics*, *120*, 10,607–10,621. https://doi.org/10.1002/2015JA021819

Wang, H., Lhr, H., & Ma, S. Y. (2005). Solar zenith angle and merging electric field control of field-aligned currents: A statistical study of the Southern Hemisphere. *Journal of Geophysical Research*, *110*, A03306. https://doi.org/10.1029/2004JA010530

Wang, Y., Zhang, Q.-H., Jayachandran, P., Moen, J., Xing, Z.-Y., Chadwick, R., et al. (2018). Experimental evidence on the dependence of the standard GPS phase scintillation index on the ionospheric plasma drift around noon sector of the polar ionosphere. *Journal of Geophysical Research: Space Physics*, *123*, 2370–2378. https://doi.org/10.1002/2017JA024805

Welch, P. (1967). The use of fast Fourier transform for the estimation of power spectra: A method based on time averaging over short, modified periodograms. *IEEE Transactions on Audio and Electroacoustics*, *15*(2), 70–73. https://doi.org/10.1109/TAU.1967.1161901

Wernik, A., Secan, J., & Fremouw, E. (2003). Ionospheric irregularities and scintillation. *Advances in Space Research*, *31*(4), 971–981.

Yeh, K. C., & Liu, C.-H. (1982). Radio wave scintillations in the ionosphere. *Proceedings of the IEEE*, *70*(4), 324–360. https://doi.org/10.1109/PROC.1982.12313